Supplementary Information

X-ray photoelectron spectroscopy of high-throughput mechanically exfoliated van der Waals materials

Nuria Jiménez-Arévalo[1,*], Carlo Mariani[1,2], Fabrice Leardini[3], Francesco Pandolfi[2], Ilaria Rago[2], Riccardo Frisenda[1,*].

1 Dipartimento di Fisica, Università di Roma “La Sapienza”, 00185, Rome, Italy.

2 Istituto Nazionale di Fisica Nucleare Sezione di Roma, 00185 Rome, Italy

3 Departamento de Física de Materiales, Universidad Autónoma de Madrid, 28049 Madrid, Spain

*corresponding author: nuria.jimenezarevalo@uniroma1.it, riccardo.frisenda@uniroma1.it

Preparation of the samples

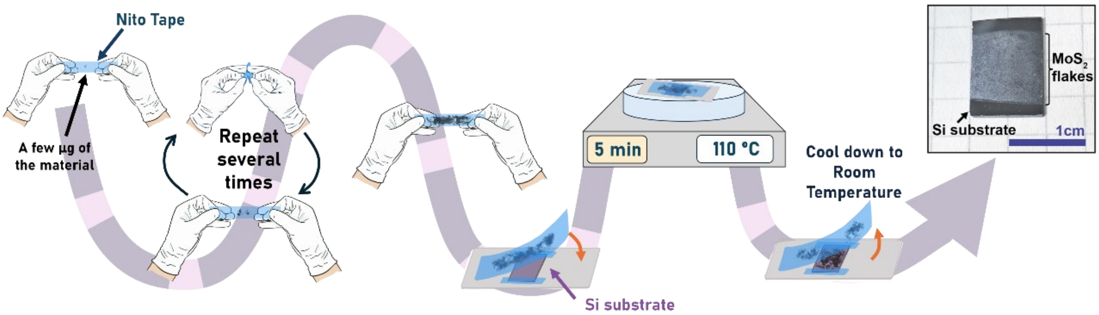

Figure S1. Schematic of the preparation technique of the samples

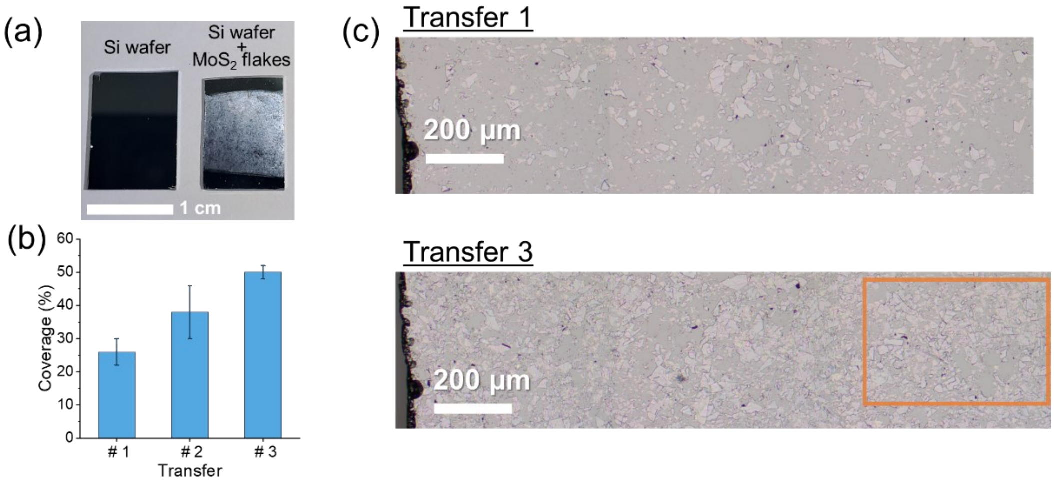

Figure S2. (a) Photograph of a Si substrate without flakes and a Si substrate with MoS_2 flakes transferred. (b) Coverage percentage after each transfer calculated by the analysis of several optical microscopy images. (c) Same region of the sample after one transfer and after three transfers. The area marked in orange corresponds with the one shown in Figure 1c.

Morphological characterization of MoS_2 and graphite flakes

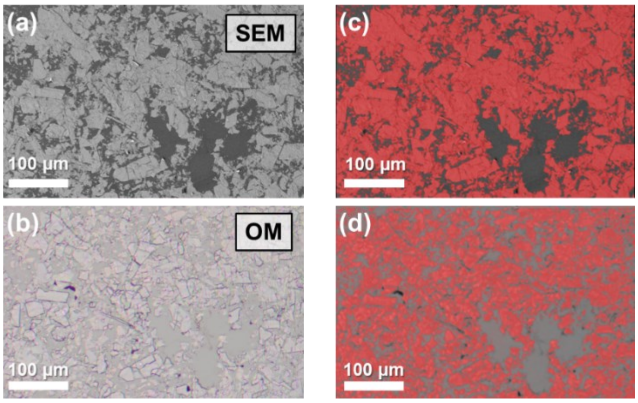

Figure S3. MoS_2 (a) SEM and (b) OM images (shown in Figures 1c and 1d), and their corresponding image analysis to determine the coverage of the flakes using Gwyddion software. In the same region, 60±5 % of coverage is obtained by the analysis of OM image and 70± 5 % for the SEM one.

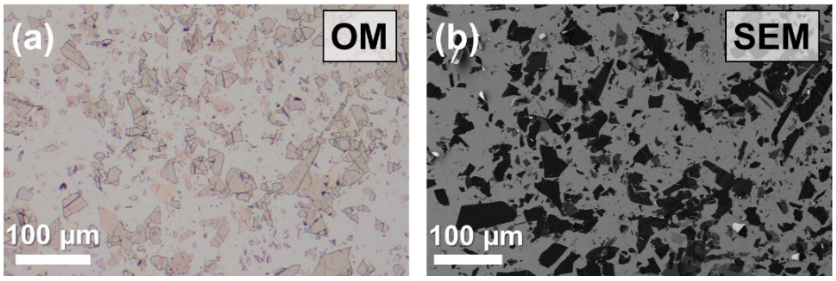

Figure S4. (a) Optical microscopy and (b) SEM image for the graphite flakes sample

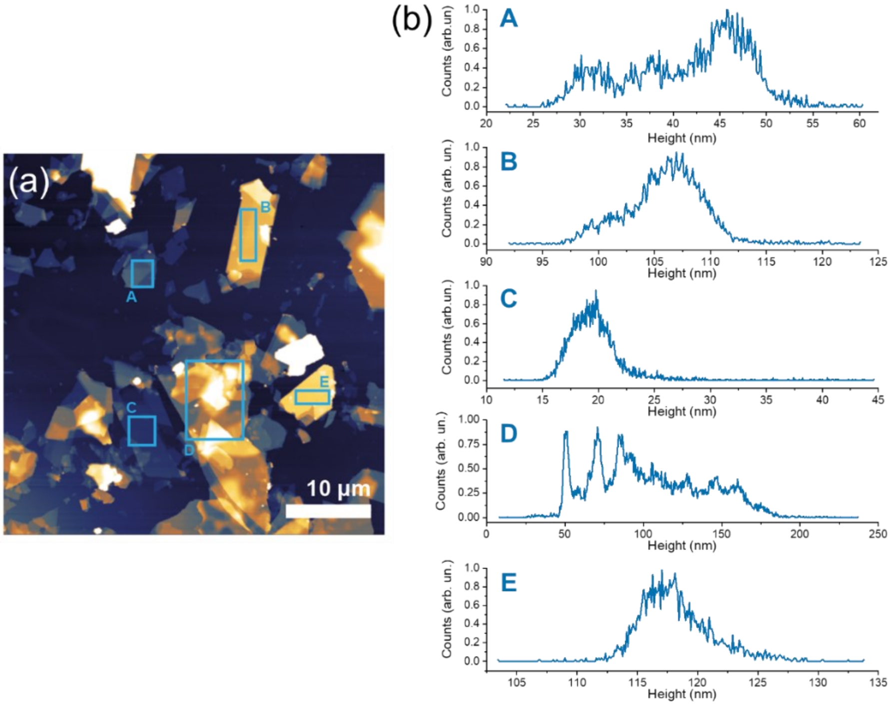

Figure S5. (a) AFM image of 45x45µm^2. (b) Height profile in the regions marked with squares and letters in (a).

XPS for MoS$_2$

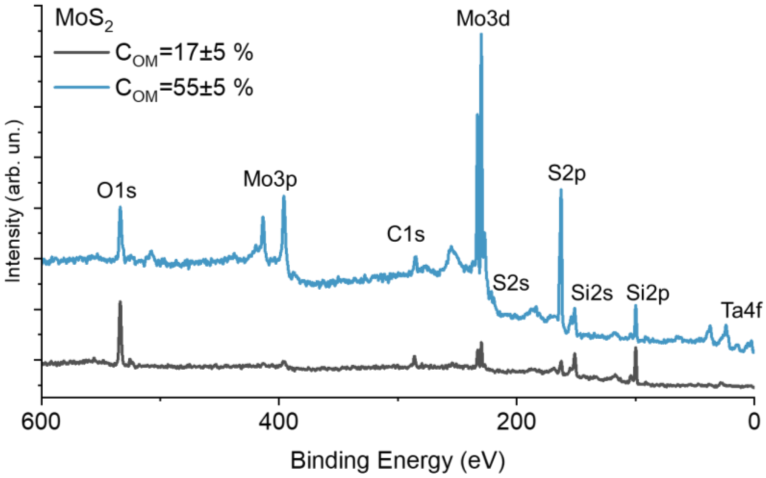

Figure S6. XPS survey spectra for two MoS$_2$ samples with a different coverage obtained by optical microscopy (C$_{OM}$). Peaks are identified as labelled in the figure.

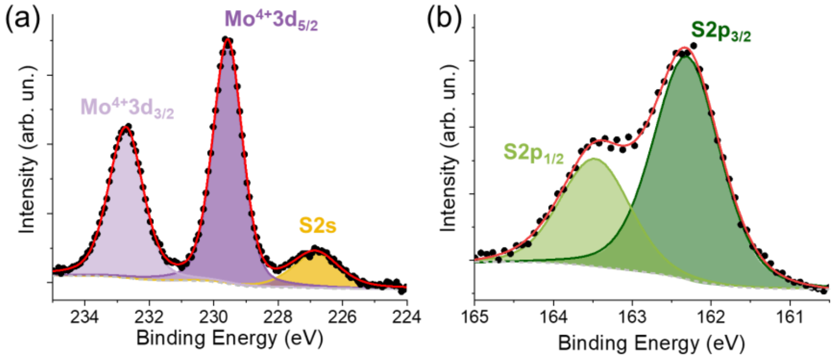

Figure S7. (a) Mo 3d and S 2s and (b) S 2p core levels of the MoS$_2$ sample with a C$_{OM}$ =(17 ±5) % coverage. Experimental data indicated with dots, total fit in red, and Shirley background with a dashed grey line. The individual peaks are coloured and their corresponding core-levels are indicated in the figure.

	Core-level	*Component core-level*	*Binding Energy (eV)*	*FWHM (eV)*	*G-L ratio*
MoS$_2$ flakes	**Mo 3d**	3d $_{3/2}$	233.0	1.2	0.2
		3d $_{5/2}$	229.8	1.1	0.3
	S 2s		227.1	1.9	0.1
	S 2p	2p $_{1/2}$	163.8	1.0	0.4
		2p $_{3/2}$	162.6	1.1	0.4
	Si 2p	2p $_{1/2}$	100.3	0.9	0.7
		2p $_{3/2}$	99.7	1.0	0.3
		SiO$_2$	104.0	1.8	0.1

Table S1. Fitting parameters for the MoS$_2$ flakes sample. Position (BE), full width at half maximum (FWHM), and Gaussian-Lorentzian (G-L) ratio.

Discussion about the coverage obtained by the analysis of the survey and background selection.

The analysis of the background in the XPS survey scans provides valuable insights into the quantitative analysis of XPS from nanostructures on surfaces, a factor often overlooked. In our case, the sample geometry is well-known, consisting of island of the 2D material under investigation, with micrometric lateral sizes and thicknesses ranging from 20 to 200 nm. These islands partially cover the Si substrate, which has a native oxide layer on top (oxide thickness < 2nm as estimated by optical reflectance) (see Figure 1 in the main text). The geometry is schematically illustrated in Figure S8.

The largest electron mean free path (λ) possible in our experiment is 2 nm, with most of the signal having λ of 1 nm or less [1,2]. Therefore, for thin films thicker than 5-10 nm (corresponding to 5λ), we do not expect any contribution from inelastically scattered electrons photoemitted by the substrate in the regions covered by the islands.

Visual inspection of the MoS_2 and Gr XPS survey spectra (see Figure S9 a,b) reveals differences in the background below the Mo, S, C and Si peaks, which is due to the different depth distributions of the atoms. As discussed in references [3] and [4], and using the peak shape nomenclature discussed in those references, the following conclusions can be drawn: Mo and S peaks, as well as the C peak, are *"type a"* peaks (see Figures S9c,d), meaning that photoelectrons emitted from these atoms are not attenuated by any overlying layer of different material, as evidenced by negatively sloped background decreasing for binding energies larger than the Mo, S and C elastic peaks. In contrast, Si atoms are attenuated by the native oxide layer on top (Figures S9c,d), showing only a flat background.

These attenuation effects, evident in the background, must be considered when fitting to calculate peak areas to obtain coverage. Figure S9a and b show the survey spectra for MoS_2 and Gr, with the background for some significant core-levels as indicated as in the legend. For all of them a Shirley plus a slope-background (defined by Herrera-Gomez in reference [5]), has been applied. In the case of Mo, S and C core-levels, a negative slope is required to accurately fit the experimental inelastic tail.

By subtracting that background to each peak, the area of each peak has been obtained, which has permitted us to estimate the coverage by applying the following equations (equations 1 and 2) where the area of each core level is defined as the area of the peak divided by the corresponding cross section σ ($A_{core\ level} = \frac{Peak\ Area}{\sigma_{core\ levl}}$)

$$C_{XPS}(MoS_2) = \frac{A_{MoS_2}}{A_{TOTAL}} = \frac{A_{Mo3d} + A_{Mo3p} + A_{S2p} + A_{S2s}}{A_{Si2s} + A_{Si2p} + A_{O1s} + A_{Mo3d} + A_{Mo3p} + A_{S2p} + A_{S2s}} \quad (1)$$

$$C_{XPS}(Gr) = \frac{A_{Gr}}{A_{TOTAL}} = \frac{A_{C1s}}{A_{Si2s} + A_{Si2p} + A_{O1s} + A_{C1s}} \quad (2)$$

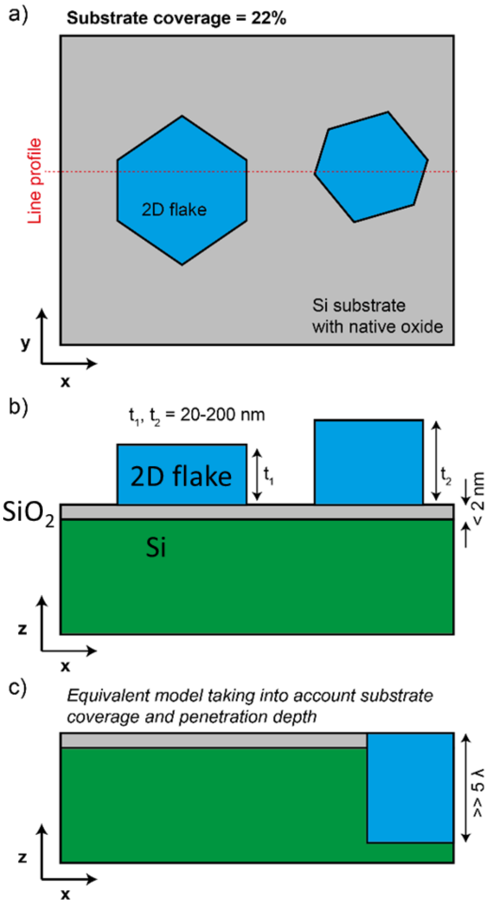

Figure S8. Schematic model of the sample geometry in top (a) and lateral view (b). c) Equivalent geometry taking into account the substrate coverage with 2D flakes (22%) and the photoelectrons penetration depth.

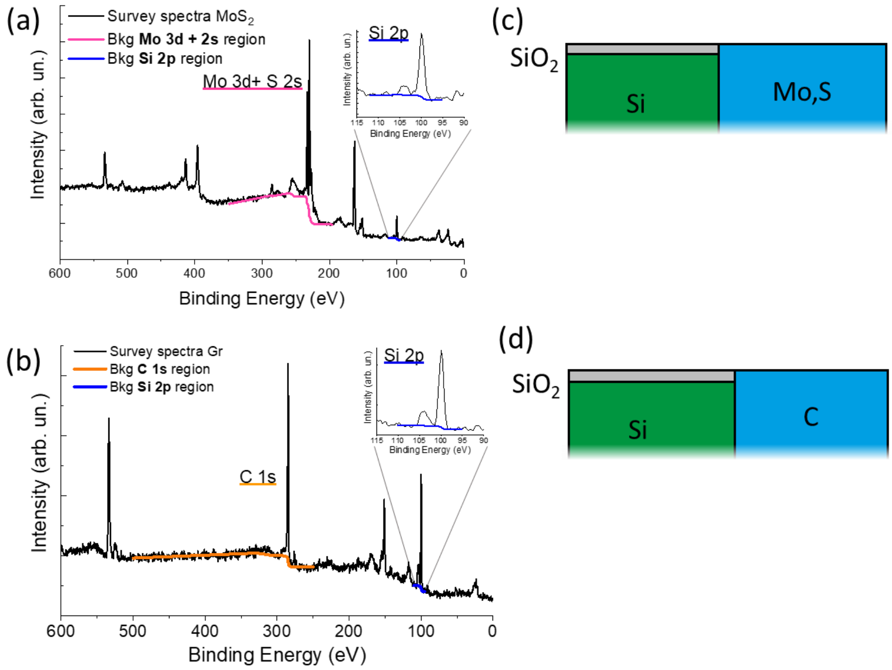

Figure S9. Survey spectra for MoS_2 (a) and graphite (b) flakes, deposited on a Si substrate with a native oxide on top. The corresponding backgrounds as indicated in the figure have been calculated by using the sum of a Shirley and a slope-background. Panels (c) and (d) shows the schematic of the equivalent geometry for each case.

Morphological characterization for WSe_2

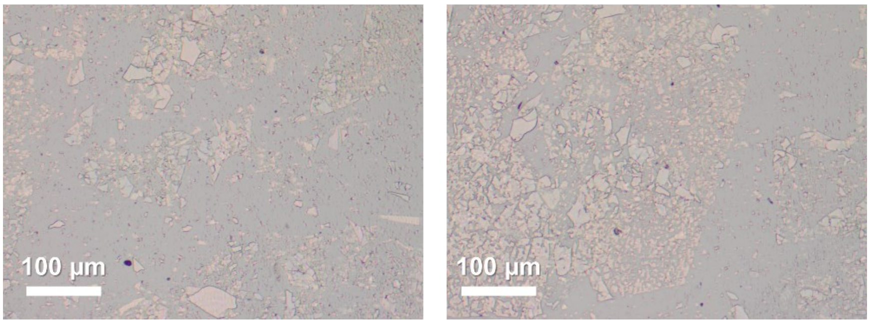

Figure S10. Two optical microscopy images recorded in two different regions of sample WSe_2.

XPS for Gr-flakes compared to HOPG

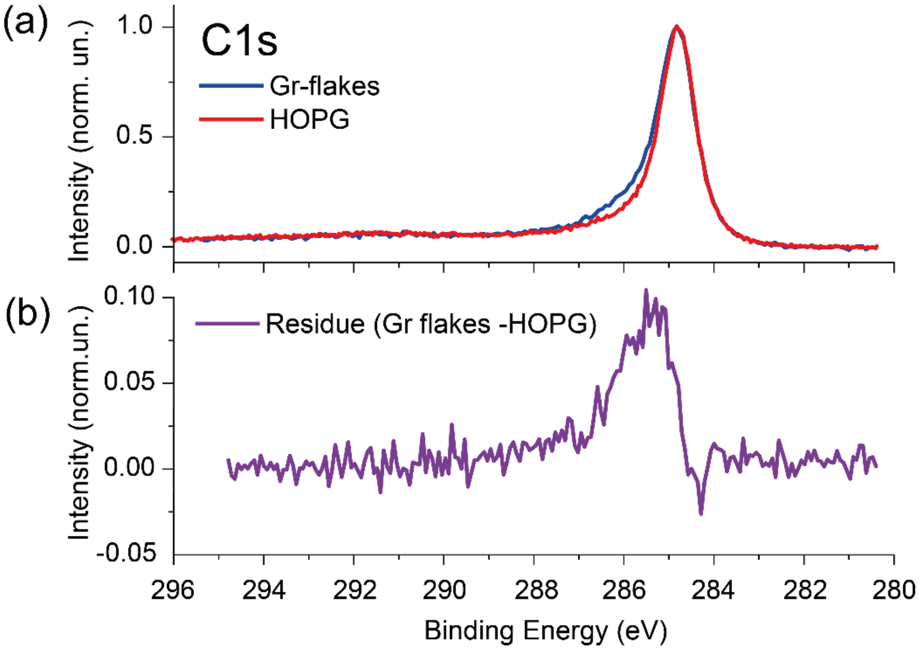

Figure S11. (a) C 1s core level for the graphite flakes and a highly oriented pyrolytic graphite (HOPG) sample recorded in the same system. (b) Residual difference signal between the C 1s spectra of the Gr-flakes and the HOPG.

XPS fitting parameters for Gr and WSe$_2$-flakes

	Core-level	*Component core-level*	*Binding Energy (eV)*	*FWHM (eV)*	*G-L ratio*
Gr flakes	**C1s**	sp^2	284.8	1.0	0.7
		C-O	285.9	1.8	0.9
		π-plasmon	291.3	2	0.1

Table S2. Fitting parameters for the Gr flakes sample. Position (BE), full width at half maximum (FWHM), and Gauss-Lorentz (G-L) ratio.

	Core-level	*Component core-level*	*Binding Energy (eV)*	*FWHM (eV)*	*G-L ratio*
WSe$_2$ flakes	**W 4f**	4f $_{7/2}$	32.6	0.9	0.5
		4f $_{5/2}$	34.7	1.0	0.4
	Se 3d	3d $_{5/2}$	54.8	1.0	0.6
		3d $_{3/2}$	55.7	0.9	0.4

Table S3. Fitting parameters for the WeS$_2$ flakes sample. Position (BE), full width at half maximum (FWHM), and Gauss-Lorentz (G-L) ratio.

XPS for FePS$_3$

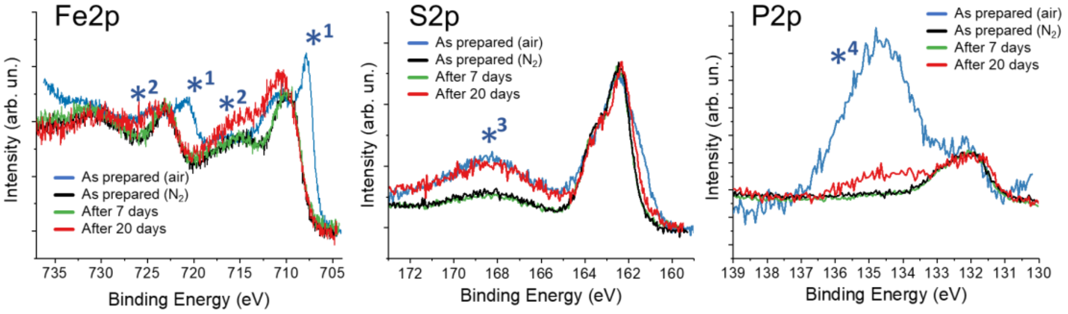

Figure S12. Fe 2p, P 2p, and S 2p core levels for the FePS$_3$ flakes transferred in air, in the inert atmosphere of N$_2$, and that last sample after 7 and 20 days stored in air. ($*^1$) Peaks associated with pure iron [6], ($*^2$) peaks due to iron oxide [7,8], ($*^3$) peaks of sulfates/ sulfur oxide [9–11], and ($*^4$) peaks due to phosphorous oxide [12–14].

	Core-level	*Component core-level*	*Binding Energy (eV)*	*FWHM (eV)*	*G-L ratio*
FePS$_3$ flakes	**Fe2p**	Fe^{2+} 2p $_{3/2}$	709.2	2.3	0.05
		Fe^{2+} 2p $_{1/2}$	722.7	2	0.8
		Fe^{3+} 2p $_{3/2}$	710.9	2.5	0.05
		Fe^{3+} 2p $_{1/2}$	723.7	2.3	1.0
		Sat 1	714.7	4.2	0.05
		Sat 2	730.8	5	0.5
	S2p	2p 3/2	162.4	1.2	0.4
		2p 1/2	163.5	1.3	0.05
		sulfates	168.5	3.3	0.05
	P2p	2p $_{3/2}$	131.8	1.1	0.8
		2p $_{1/2}$	132.7	1.3	0.05

Table S4. Fitting parameters for the FePS$_3$ flakes sample. Position (BE), full width at half maximum (FWHM), and Gauss-Lorentz (G-L) ratio.

References

1. Tanuma, , S., Powell, C. J. & Penn, D. R. Calculations of electron inelastic mean free paths. IX. Data for 41 elemental solids over the 50 eV to 30 keV range. *Surface and Interface Analysis* **43**, 689–713 (2011).

2. Powell, C. J. Practical guide for inelastic mean free paths, effective attenuation lengths, mean escape depths, and information depths in x-ray photoelectron spectroscopy. *Journal of Vacuum Science & Technology A: Vacuum, Surfaces, and Films* **38**, 023209 (2020).

3. Tougaard, S. Improved XPS analysis by visual inspection of the survey spectrum. *Surface and Interface Analysis* **50**, 657–666 (2018).

4. Tougaard, S. Practical guide to the use of backgrounds in quantitative XPS. *Journal of Vacuum Science & Technology A* **39**, 011201 (2021).

5. Herrera-Gomez, A., Bravo-Sanchez, M., Aguirre-Tostado, F. S. & Vazquez-Lepe, M. O. The slope-background for the near-peak regimen of photoemission spectra. *J Electron Spectros Relat Phenomena* **189**, 76–80 (2013).

6. Biesinger, M. C. *et al.* Resolving surface chemical states in XPS analysis of first row transition metals, oxides and hydroxides: Cr, Mn, Fe, Co and Ni. *Appl Surf Sci* **257**, 2717–2730 (2011).

7. He, Y. *et al.* Iron-Based Oxygen Scavengers on Mesoporous Silica Nanospheres. *ACS Omega* **8**, 21689–21695 (2023).

8. Swiatkowska-Warkocka, Z., Kawaguchi, K., Wang, H., Katou, Y. & Koshizaki, N. Controlling exchange bias in Fe3O4/FeO composite particles prepared by pulsed laser irradiation. *Nanoscale Res Lett* **6**, 226 (2011).

9. Ding, Y. *et al.* Facile Synthesis of FePS3 Nanosheets@MXene Composite as a High-Performance Anode Material for Sodium Storage. *Nanomicro Lett* **12**, 54 (2020).

10. Wang, H. *et al.* An exfoliated iron phosphorus trisulfide nanosheet with rich sulfur vacancy for efficient dinitrogen fixation and Zn-N2 battery. *Nano Energy* **81**, 105613 (2021).

11. Ma, Y. *et al.* Rational design of few-layer FePS3 nanosheets@N-doped carbon composites as anodes for sodium-ion batteries. *Chemical Engineering Journal* **427**, 130882 (2022).

12. Qin, Q. *et al.* A Tannic Acid–Derived N-, P-Codoped Carbon-Supported Iron-Based Nanocomposite as an Advanced Trifunctional Electrocatalyst for the Overall Water Splitting Cells and Zinc–Air Batteries. *Adv Energy Mater* **9**, 1803312 (2019).

13. Mukherjee, D., Austeria, P. M. & Sampath, S. Two-Dimensional, Few-Layer Phosphochalcogenide, FePS3 : A New Catalyst for Electrochemical Hydrogen Evolution over Wide pH Range. *ACS Energy Lett* **1**, 367–372 (2016).

14. Chen, G. *et al.* Efficient and Stable Bifunctional Electrocatalysts Ni/NixMy (M = P, S) for Overall Water Splitting. *Adv Funct Mater* **26**, 3314–3323 (2016).